

Parameterization of contrail radiative properties for climate studies

Yu Xie,¹ Ping Yang,¹ Kuo-Nan Liou,² Patrick Minnis,³ and David P. Duda⁴

Received 27 September 2012; revised 6 November 2012; accepted 9 November 2012; published 20 December 2012.

[1] The study of contrails and their impact on global climate change requires a cloud model that statistically represents contrail radiative properties. In this study, the microphysical properties of global contrails are statistically analyzed using collocated Moderate Resolution Imaging Spectroradiometer (MODIS) and Cloud Aerosol Lidar with Orthogonal Polarization (CALIOP) observations. The MODIS contrail pixels are detected using an automated contrail detection algorithm and a manual technique using the brightness temperature differences between the MODIS 11 and 12 μm channels. The scattering and absorption properties of typical contrail ice crystals are used to determine an appropriate contrail model to minimize the uncertainties arising from the assumptions in a particular cloud model. The depolarization ratio is simulated with a variety of ice crystal habit fractions and matched to the collocated MODIS and CALIOP observations. The contrail habit fractions are determined and used to compute the bulk-scattering properties of contrails. A parameterization of shortwave and longwave contrail optical properties is developed for the spectral bands of the Rapid Radiative Transfer Model (RRTM). The contrail forcing at the top of the atmosphere is investigated using the RRTM and compared with spherical and hexagonal ice cloud models. Contrail forcing is overestimated when spherical ice crystals are used to represent contrails, but if a hexagonal ice cloud model is used, the forcing is underestimated for small particles and overestimated for large particles in comparison to the contrail model developed in this study. **Citation:** Xie, Y., P. Yang, K.-N. Liou, P. Minnis, and D. P. Duda (2012), Parameterization of contrail radiative properties for climate studies, *Geophys. Res. Lett.*, 39, L00F02, doi:10.1029/2012GL054043.

1. Introduction

[2] Air transport has become vitally important for both social and economic activities. According to the 2010 Transportation Statistics Annual Report [*U.S. Department of Transportation*, 2011], the number of domestic and international passengers on flights to and from the United States

had risen from 442 million in 1995 to 701 million in 2009. Air travel and fuel consumption are expected to continue to increase yearly by 5% and 3%, respectively, until 2026 [*Nygren et al.*, 2009]. Rigorous methods will be required to study the rapid growth of worldwide air transport and to determine the current and potential effect on global climate change. The line-shaped artificial clouds often visible behind cruising aircraft are known as contrails and are initially triggered by the water vapor within aircraft engine exhaust. The correlation between the exhaust particles and other atmospheric parameters is important to climatologists studying the aviation climate impact.

[3] Contrails reflect incoming solar radiation and absorb infrared radiation emitted from the Earth and atmosphere, and the effect on the global energy budget is similar to natural clouds [*Lee et al.*, 2009; *Penner et al.*, 1999]. *Liou et al.* [1998] analyzed the optical properties of contrails using the contrail particle size distributions obtained during the Subsonic Aircraft: Contrail and Cloud Effects Special Study (SUCCESS) and an experiment sponsored by the U.S. Department of Energy carried out over northern Oklahoma and southern Kansas. The results suggested that contrail particles could be modeled using a mixture of 50% bullet rosettes, 30% hollow columns, and 20% plates. However, most previous studies reported in the literature, concerning contrail radiative forcing and its impact on climate change, almost exclusively used natural ice cloud models to represent the optical properties of contrails. Commercial aircraft cruise altitudes correspond to extremely low atmospheric temperatures at which the water vapor in aircraft engine exhaust mixes with the ambient air, condenses, and immediately freezes into ice crystals. *Marquart et al.* [2003] employed a contrail parameterization scheme for the version 4 European Center/Hamburg General Circulation Model (ECHAM4) in which spherical and nonspherical ice particles were assumed. The modeling effort yielded an average global value of contrail radiative forcing of 2.8 mW m^{-2} for 1992 when spherical particles were used, substantially smaller than the estimate produced by the Intergovernmental Panel on Climate Change (IPCC) [*Penner et al.*, 1999]. *Rap et al.* [2010] used hexagonal cylinders to represent contrails whose shortwave and longwave radiative fluxes were computed by Hadley Center climate model HadGEM2. Based on the computation, the global mean contrail radiative forcing increased from 19.6 mW m^{-2} in 2002 to 33.2 mW m^{-2} when contrails were represented by spherical ice crystals.

[4] *In situ* measurements of contrail microphysics are extremely difficult and rare, especially during the early phase of contrail formation. From the small number of observations conducted by *Goodman et al.* [1998], the majority of particles within contrails were found to be nonspherical ice crystals. In climate models involving contrails, the ice crystal habit and size distributions should be specified, and may not

¹Department of Atmospheric Sciences, Texas A&M University, College Station, Texas, USA.

²Joint Institute for Earth System Science and Engineering and Department of Atmospheric and Oceanic Sciences, University of California, Los Angeles, California, USA.

³Science Directorate, NASA Langley Research Center, Hampton, Virginia, USA.

⁴Science Systems and Applications, Inc., Hampton, Virginia, USA.

Corresponding author: P. Yang, Department of Atmospheric Sciences, Texas A&M University, College Station, TX 77843, USA. (pyang@tamu.edu)

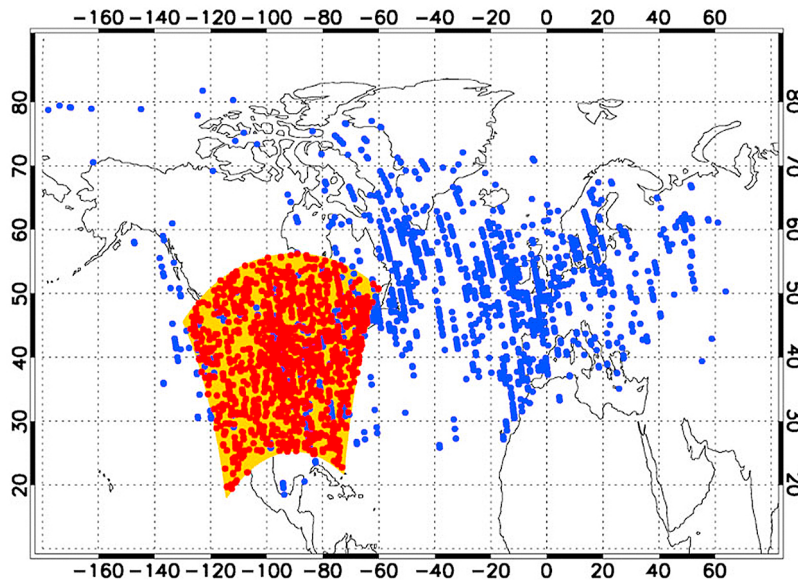


Figure 1. Geographical contrail locations. Blue dots: 2007 contrails identified by MODIS data and collocated to CALIOP. Yellow dots: contrails of July-December 2006 detected by the CDA. Red dots: Collocated MODIS and CALIOP data for July-December 2006.

be the same as in natural ice clouds due to the unique physical mechanism of contrail formation. The microphysical properties of global contrails can be statistically investigated using satellite observations. Our objective is to summarize the satellite observations of contrails and to develop a global contrail scattering property parameterization, which can be used in studies of climate change. The uncertainties arising from simulations of contrail radiative forcing using ice cloud models are also discussed.

2. Contrail Data

[5] *Iwabuchi et al.* [2012] investigated the physical and optical properties of contrails using the collocated Moderate Resolution Imaging Spectroradiometer (MODIS) and Cloud Aerosol Lidar with Orthogonal Polarization (CALIOP) data for the years of 2007 and 2009. The contrails were manually detected from MODIS brightness temperature differences (BTD) between the 11 and 12 μm channels, because, in comparison to other clouds, contrails are generally brighter and featured by their linear shapes. The detection scheme has the ability to determine contrail ages and to exclude cases where contrails are crowded or overlapped by clouds. The contrail pixels are collocated to CALIOP data, which produces the optical and microphysical properties of contrails. A more efficient method to detect contrails, however, is an automated contrail detection algorithm (CDA), which defines thresholds in order to recognize pixels that appear as lines in the normalized 11–12 μm BTD image [e.g., *Minnis et al.*, 2005].

[6] We have taken advantage of the contrail data from the preceding two detection methods to increase the sample size and to statistically minimize the regional and limiting preferences from the use of only one algorithm. The CDA and the resulting contrail detections using MODIS data have been described by *Duda et al.* [2011]. The CDA contrail pixels are collocated with CALIOP data in order to infer the contrail shown in *Iwabuchi et al.* [2012]. The geographical locations of the identified contrails are illustrated in Figure 1, where the

blue dots indicate 2007 contrails manually identified from MODIS data and collocated with CALIOP data. The yellow dots are contrails detected by the CDA for July-December 2006, while the red dots represent the collocated MODIS and CALIOP data for July-December 2006. The blue dots over the continental United States (US) are obscured by yellow and red dots. The CDA is found to provide more contrail data compared with the manual detection algorithm (5780 collocated pixels for July-December 2006 vs. 1484 collocated pixels for the entire 2007 year). However, the 2006 CDA data are concentrated over the continental US and its surrounding areas; thus, the 2006 and 2007 combined data are more meaningful for global scale contrail studies. In the current study, contrail data from July-December 2006 and the whole year of 2007 are used.

3. Contrail Model and Optical Property Parameterization

[7] *In situ* measurements of aviation emissions suggest that the major elements in contrail and contrail-cirrus are ice crystals with irregular particle shapes [*Goodman et al.*, 1998]. In previous studies of global climate change, specific cloud models were used to represent all ice clouds in General Circulation Models (GCMs). The cloud models require the explicit distribution of ice crystal size and morphological habit, and are unable to exactly define all the realistic ice clouds within the atmosphere. Selecting a proper cloud model can minimize the uncertainties caused by nonconformity of the model's ice crystals to the observations. Following the study of *Iwabuchi et al.* [2012], we developed an algorithm to determine an appropriate contrail model to minimize the uncertainties. In the algorithm, we matched the contrail depolarization ratio values from the 2006 and 2007 satellite data to the simulations for single-backscattering events at a wavelength of 0.532 μm . The simulated contrail depolarization ratio can be defined by

$$\delta = \frac{\langle P_{11}(\pi) \rangle - \langle P_{22}(\pi) \rangle}{\langle P_{11}(\pi) \rangle + \langle P_{22}(\pi) \rangle}, \quad (1)$$

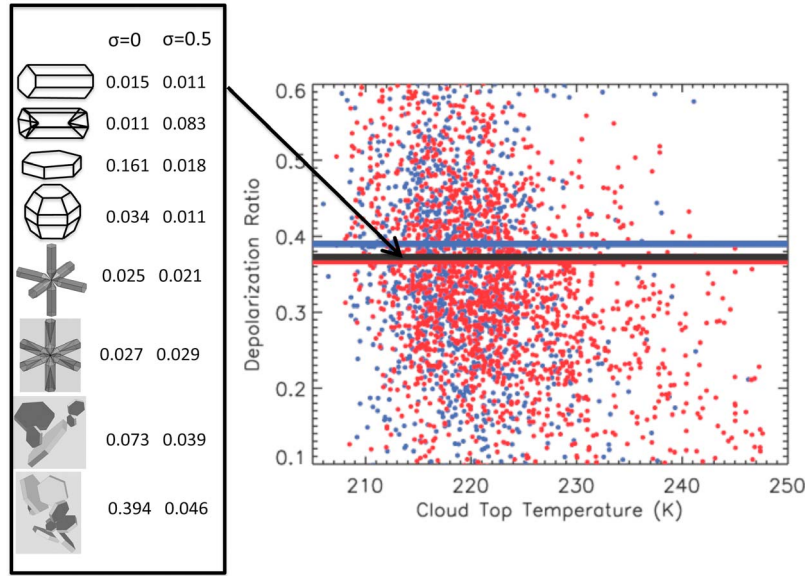


Figure 2. Depolarization ratios for July-December 2006 (red) and 2007 (blue) as a function of contrail temperature. The RMS tilt, σ , of the individual facets on ice crystal surfaces is used to represent ice crystal surface roughness. $\sigma = 0$ and 0.5 are related to smooth and severely rough surfaces [Yang *et al.*, 2008a].

where P_{11} and P_{22} are two elements of the scattering phase matrix, π represents the backscattering direction, and $\langle \rangle$ denotes the contrail bulk scattering properties averaged over various ice crystal habits. The single-scattering properties of ice crystals are computed using a synergetic combination of the discrete dipole approximation (DDA) method [Yurkin *et al.*, 2007] and the Improved Geometric Optics Method (IGOM) [Yang and Liou, 1996].

[8] For each collocated contrail pixel, a set of the most appropriate habit fractions is determined by assuming that the effective contrail particle diameter D_e is $20 \mu\text{m}$. In the simulation of contrail depolarization ratio, a slight sensitivity to contrail particle size was shown for habit mixture models [Iwabuchi *et al.*, 2012]. The contrail particle size distribution, $n(D)$, follows that reported by Iwabuchi *et al.* [2012]:

$$n(D) = \frac{(D/\nu)^{\alpha-1} \exp(-D/\nu)}{\nu \Gamma(\alpha)}, \quad (2)$$

where D represents the maximum dimension of an ice crystal, $\Gamma(\alpha)$ is the Gamma function, and

$$\alpha + 2 = 6.01 \times \nu^{-0.137}. \quad (3)$$

The overall contrail habit fractions are then given by

$$F_i = \frac{1}{M} \sum_{j=1}^M f_{ij} \quad (i = 1, 2, \dots, N), \quad (4)$$

where M represents the number of the collocated contrail pixels, N denotes the number of ice crystal habits, and f is the optimal fraction of each ice habit determined for each pixel.

[9] Figure 2 (left) shows the habit fractions determined using the depolarization ratios found during July-December 2006 and 2007. The contrail ice crystals are assumed to be hexagonal columns, hollow columns, hexagonal plates, droxtals, bullet rosettes, hollow bullet rosettes [Yang *et al.*, 2008b], and aggregates of plates [Xie *et al.*, 2011] with either smooth or roughened surfaces. Among the 16 ice crystal habits, the smooth surfaced aggregates of plates are the

most frequent particles. The overall fraction of all aggregates is above 0.5. Figure 2 (right) shows the depolarization ratios from satellite observations of July-December 2006 and 2007 as a function of contrail temperature. The solid lines in the figure indicate the depolarization ratios simulated using the single-scattering properties of ice crystals and the determined ice crystal habit fractions. The red, blue, and black lines, respectively, denote simulations from the 2006, 2007, and combined data. The figure indicates that the simulated depolarization ratios are consistent with satellite data, while the combined data lie between the 2006 and 2007 data. Thus, the determined particle habit fraction is slightly dependent on the geographical location and observing time. In addition, the simulated depolarization ratios were calculated in the most densely observed region, implying that the determined habit fractions can lead to the smallest bias when idealized models are used to estimate the contrail radiative forcing. The habit fraction determined from the combined 2006 and 2007 contrail data is used to represent contrail properties.

[10] After the contrail model is determined, the contrail bulk-scattering properties can be written in the form

$$\langle Q_{ext} \rangle = \frac{\int_{\lambda_{\min}}^{\lambda_{\max}} \int_{D_{\min}}^{D_{\max}} \left[\sum_{i=1}^N F_i \sigma_{ext}(\lambda, D) \right] n(D) S(\lambda) dD d\lambda}{\int_{\lambda_{\min}}^{\lambda_{\max}} \int_{D_{\min}}^{D_{\max}} \left[\sum_{i=1}^N F_i A_i(D) \right] n(D) S(\lambda) dD d\lambda}, \quad (5)$$

$$\langle \omega \rangle = \frac{\int_{\lambda_{\min}}^{\lambda_{\max}} \int_{D_{\min}}^{D_{\max}} \left[\sum_{i=1}^N F_i \sigma_s(\lambda, D) \right] n(D) S(\lambda) dD d\lambda}{\int_{\lambda_{\min}}^{\lambda_{\max}} \int_{D_{\min}}^{D_{\max}} \left[\sum_{i=1}^N F_i \sigma_{ext}(\lambda, D) \right] n(D) S(\lambda) dD d\lambda}, \quad (6)$$

$$\langle g \rangle = \frac{\int_{\lambda_{\min}}^{\lambda_{\max}} \int_{D_{\min}}^{D_{\max}} \left[\sum_{i=1}^N F_i g(\lambda, D) \sigma_s(\lambda, D) \right] n(D) S(\lambda) dD d\lambda}{\int_{\lambda_{\min}}^{\lambda_{\max}} \int_{D_{\min}}^{D_{\max}} \left[\sum_{i=1}^N F_i \sigma_s(\lambda, D) \right] n(D) S(\lambda) dD d\lambda}, \quad (7)$$

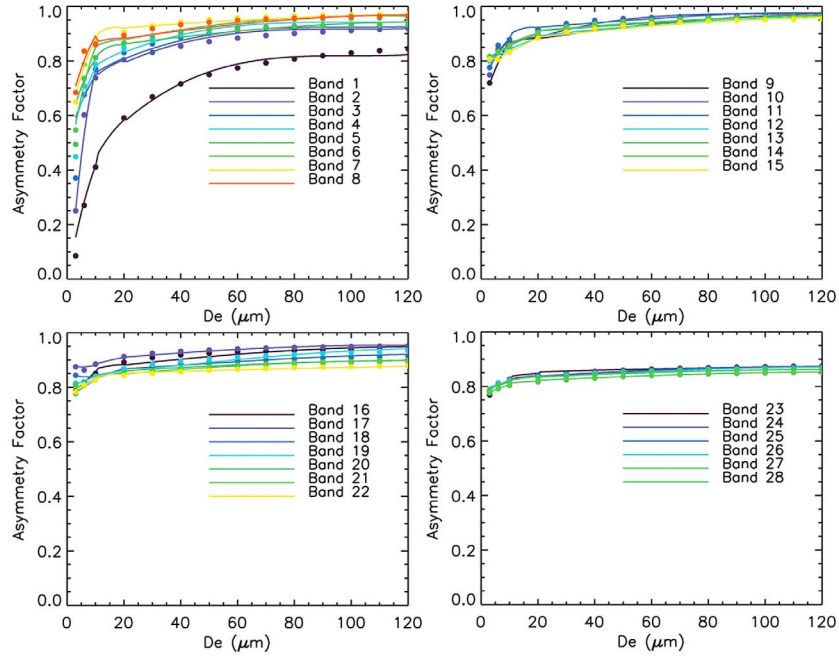


Figure 3. Computed asymmetry factor of contrail (dotted lines) and from the parameterization (solid lines).

where $\langle Q_{ext} \rangle$, $\langle \omega \rangle$, and $\langle g \rangle$, are, respectively, the extinction efficiency, the single-scattering albedo, and the asymmetry factor; σ_s and σ_{ext} denote the scattering and extinction cross sections; and, $S(\lambda)$ represents the spectral solar irradiance. For infrared wavelengths, $S(\lambda)$ is the Planck function at the point the contrail temperature, $T = 218 \text{ K}$, is the median value determined from the above observations.

[11] For climate studies, the contrail scattering properties are parameterized following the spectral bands defined in the Rapid Radiative Transfer Model (RRTM) [Mlawer *et al.*, 1997; Oreopoulos and Barker, 1999], whose GCM application (RRTMG) has been extensively applied to global and regional climate models. The contrail bulk-scattering properties can then be specified by

$$\langle \beta \rangle / IWC = \sum_{n=0}^5 a_n \left(\frac{1}{D_e} \right)^n \quad (8)$$

$$IWC = \rho_{ice} \int_{D_{min}}^{D_{max}} \left[\sum_{i=1}^N F_i V_i(D) \right] n(D) dD \quad (9)$$

$$\langle \beta_a \rangle / IWC = \sum_{n=-1}^4 b_n \left(\frac{1}{D_e} \right)^n \quad (10)$$

$$1 - \langle \omega \rangle = \sum_{n=0}^5 c_n D_e^n \quad (11)$$

$$\langle g \rangle = \begin{cases} \sum_{n=0}^3 d_n D_e^n, & \text{for } D_e \leq 10 \mu\text{m} \\ r \sum_{n=0}^3 d_n D_e^n + (1-r) \sum_{n=0}^3 e_n D_e^n, & \text{for } 10 \mu\text{m} < D_e < 20 \mu\text{m} \\ \sum_{n=0}^3 e_n D_e^n, & \text{for } D_e \geq 20 \mu\text{m} \end{cases} \quad (12)$$

where ρ_{ice} is the density of ice crystals, r is a function of RRTM band giving $\langle g \rangle$ a smooth transition from $D_e = 10$ to

$20 \mu\text{m}$, IWC is the ice water content, and β and β_a are the extinction and absorption coefficients, respectively.

[12] Figure 3 shows the simulated contrail asymmetry factor values and their counterparts derived from the parameterization for RRTM bands where Bands 1–15 are for infrared wavelengths and 16–28 are for visible wavelengths. Band 29 of RRTM is not compared with Bands 23–28 in Figure 3 because it is in the infrared region. It can be seen from Figure 3 that the asymmetry factor of contrail particles is sensitive to RRTM bands in the infrared region. For each band, the asymmetry factor increases with contrail particle size due to the increase of diffraction compared to the scattering of light by contrail particles. The contrail scattering properties are in good agreement with those determined from the parameterization. Thus, the parameterization is a convenient and accurate way to implement the contrail scattering properties in climate models studying global climate change.

4. Sensitivity of Contrail Forcing to Contrail Model

[13] As previously mentioned, the GCMs normally use ice cloud models to represent contrails. In the RRTM, the optical properties of ice clouds are computed using spherical or non-spherical ice crystals assumed to be hexagonal and randomly oriented in space [Fu, 1996]. In our study, the contrail scattering properties are applied to the RRTM for radiative forcing computations using the monochromatic molecular absorption in the atmosphere computed from the 1976 U.S. Standard Atmosphere. Contrails, having a fractional cover averaging 0.1%, are represented by a single cloud layer between 10 and 10.5 km. By using the RRTM, the solar and infrared fluxes can be simulated and their respective contrail forcing are defined by

$$C_{SW} = F_{clear}^{\uparrow} - F_{contrail}^{\uparrow} \quad (13)$$

$$C_{LW} = F_{contrail}^{\downarrow} - F_{contrail}^{\uparrow} - F_{clear}^{\downarrow} + F_{clear}^{\uparrow}, \quad (14)$$

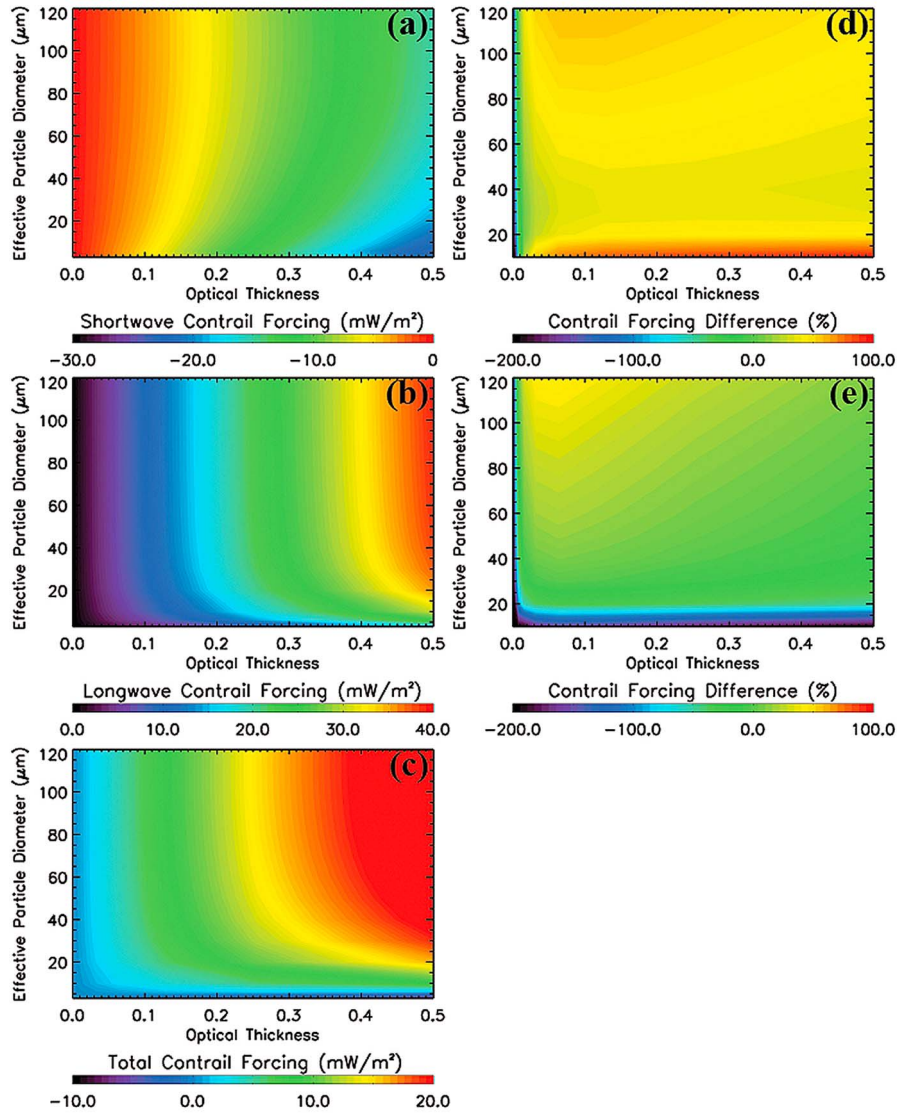


Figure 4. (a) Shortwave, (b) longwave, and (c) total contrail radiative forcing at the TOA. Contrail radiative forcing differences, (d) between using the scattering properties of contrail and spherical particles ($\frac{C_t^{\text{Sphere}} - C_t^{\text{Contrail}}}{C_t^{\text{Contrail}}} \times 100\%$), and (e) between using the scattering properties of contrail and ice cloud particles ($\frac{C_t^{\text{Ice}} - C_t^{\text{Contrail}}}{C_t^{\text{Contrail}}} \times 100\%$).

where F indicates the upwelling and downwelling fluxes at TOA for clear sky or contrail-affected conditions. The total contrail forcing can then be determined by using 12 daytime hours of solar radiation.

[14] Figures 4a–4c illustrate the shortwave, longwave and total contrail forcings at TOA, respectively, when the contrail particle size and optical depth vary within their typical values. From the simulation, the shortwave contrail forcing increases with contrail particle size but decreases with the increase of contrail optical thickness. For longwave radiation, the positive value of contrail forcing increases with both contrail particle size and optical thickness. From the results of Figure 4c, contrails generally have a slight warming effect at TOA. However, a cooling effect is evident when the contrail is extremely thin or composed of small ice crystals. Contrail forcing increases with contrail particle size and optical depth and can reach a value as large as 20 mWm^{-2} for a globally averaged contrail fraction of 0.1%. The effects of overlapped natural clouds and diurnal

and seasonal cycles of contrails have been excluded in the current simulation, which deserve further study. Figure 4d compares contrail forcing differences between spherical and contrail models. The scattering properties of spherical ice crystals have been parameterized by *Key and Schweiger* [1998]. We show that the total contrail radiative forcing is overestimated by using a parameterization of spherical particles. The overestimation becomes pronounced as D_e reaches and exceeds $\sim 10 \mu\text{m}$. When the parameterization of ice clouds [Fu, 1996] is used (see Figure 4e), the total contrail forcing is underestimated for particles smaller than $20 \mu\text{m}$, but overestimated for particles larger than $20 \mu\text{m}$.

5. Concluding Remarks

[15] Contrail optical properties were analyzed using collocated MODIS and CALIOP data for global contrails. Simulations of single scattering by contrail particles were matched to the depolarization ratios from CALIOP data.

Both a contrail model and the parameterization of its radiative properties were developed for global climate studies. The asymmetry factors of contrail increase with contrail particle size for all RRTM bands and are in good agreement with those determined from the parameterization. Based on the contrail optical properties, aggregates of plates are found to be the most densely packed ice crystals among the typical contrail ice crystals. Contrail forcing is simulated by assuming a single contrail layer between 10 and 10.5 km with a globally averaged contrail fraction of 0.1%. The simulation indicates contrail forcing increases with contrail particle size and optical depth and can reach up to 20 mWm^{-2} . Substantial errors may occur in the estimate of contrail radiative forcing when spherical or ice cloud models are used. This potential bias in global contrail forcing estimate requires further investigation. An implementation of the contrail radiative properties in GCM radiative transfer codes is also reserved for future work.

[16] **Acknowledgments.** This work is supported by the Aviation Climate Change Research Initiative (ACCRI) sponsored by the Federal Aviation Administration (FAA) under contracts DTRT57-10-C-10016 and DTRT57-10-X-70020. The authors thank Rangasayi Halthore and S. Daniel Jacob from the FAA for overseeing the project progress and for guidance and encouragement.

[17] The Editor thanks the two anonymous reviewers for their assistance in evaluating this paper.

References

- Duda, D. P., R. Palikonda, K. Khlopenkov, T. Chee, and P. Minnis (2011), A MODIS-based contrail climatology of coverage and cloud properties, paper presented at AMS 15th Conference on Aviation, Range, and Aerospace Meteorology, Am. Meteorol. Soc., Los Angeles, Calif., 1–4 Aug.
- Fu, Q. (1996), An accurate parameterization of the solar radiative properties of cirrus clouds for climate models, *J. Clim.*, *9*(9), 2058–2082, doi:10.1175/1520-0442(1996)009<2058:AAPOTS>2.0.CO;2.
- Goodman, J., R. F. Pueschel, E. J. Jensen, S. Verma, G. V. Ferry, S. D. Howard, S. A. Kinne, and D. Baumgardner (1998), Shape and size of contrails ice particles, *Geophys. Res. Lett.*, *25*(9), 1327–1330, doi:10.1029/97GL03091.
- Iwabuchi, H., P. Yang, K. N. Liou, and P. Minnis (2012), Physical and optical properties of persistent contrails: Climatology and interpretation, *J. Geophys. Res.*, *117*, D06215, doi:10.1029/2011JD017020.
- Key, J., and A. J. Schweiger (1998), Tools for atmospheric radiative transfer: Streamer and FluxNet, *Comput. Geosci.*, *24*(5), 443–451, doi:10.1016/S0098-3004(97)00130-1.
- Lee, D. S., D. W. Fahey, P. M. Forster, P. J. Newton, R. C. Wit, L. L. Lim, B. Owen, and R. Sausen (2009), Aviation and global climate change in the 21st century, *Atmos. Environ.*, *43*, 3520–3537, doi:10.1016/j.atmosenv.2009.04.024.
- Liou, K. N., P. Yang, Y. Takano, K. Sassen, T. Charlock, and W. Arnott (1998), On the radiative properties of contrail cirrus, *Geophys. Res. Lett.*, *25*(8), 1161–1164, doi:10.1029/97GL03508.
- Marquart, S., M. Ponater, F. Mager, and R. Sausen (2003), Future development of contrail cover, optical depth, and radiative forcing: Impacts of increasing air traffic and climate change, *J. Clim.*, *16*(17), 2890–2904, doi:10.1175/1520-0442(2003)016<2890:FDOCCO>2.0.CO;2.
- Minnis, P., R. Palikonda, B. J. Walter, J. K. Ayers, and H. Mannstein (2005), Contrail properties over the eastern North Pacific from AVHRR data, *Meteorol. Z.*, *14*(4), 515–523, doi:10.1127/0941-2948/2005/0056.
- Mlawer, E. J., S. J. Taubman, P. D. Brown, M. J. Iacono, and S. A. Clough (1997), RRTM, a validated correlated-k model for the longwave, *J. Geophys. Res.*, *102*, 16,663–16,682, doi:10.1029/97JD00237.
- Nygren, E., K. Aleklett, and M. Hook (2009), Aviation fuel and future oil production scenarios, *Energy Policy*, *37*(10), 4003–4010, doi:10.1016/j.enpol.2009.04.048.
- Oreopoulos, L., and H. W. Barker (1999), Accounting for subgrid-scale cloud variability in a multi-layer 1-D solar radiative transfer algorithm, *Q. J. R. Meteorol. Soc.*, *125*, 301–330.
- Penner, J. E., D. H. Lister, D. J. Griggs, D. J. Dokken, and M. McFarland (1999), *Aviation and the Global Atmosphere*, Cambridge Univ. Press, Cambridge, U. K.
- Rap, A., P. M. Forster, A. Jones, O. Boucher, J. M. Haywood, N. Bellouin, and R. R. Leon (2010), Parameterization of contrails in the UK Met Office Climate Model, *J. Geophys. Res.*, *115*, D10205, doi:10.1029/2009JD012443.
- U.S. Department of Transportation (2011), Transportation statistics annual report 2010, report, Res. and Innovative Technol. Admin., Bur. Transp. Stat., Washington, D. C.
- Xie, Y., P. Yang, G. W. Kattawar, B. Baum, and Y. X. Hu (2011), Simulation of the optical properties of ice particle aggregates for application to remote sensing of cirrus clouds, *Appl. Opt.*, *50*, 1065–1081, doi:10.1364/AO.50.001065.
- Yang, P., and K. N. Liou (1996), Geometric-optics-integral-equation method for light scattering by nonspherical ice crystals, *Appl. Opt.*, *35*(33), 6568–6584, doi:10.1364/AO.35.006568.
- Yang, P., G. W. Kattawar, G. Hong, P. Minnis, and Y. X. Hu (2008a), Uncertainties associated with the surface texture of ice particles in satellite-based retrieval of cirrus clouds. Part I: Single-scattering properties of ice crystals with surface roughness, *IEEE Trans. Geosci. Remote Sens.*, *46*(7), 1940–1947, doi:10.1109/TGRS.2008.916471.
- Yang, P., Z. B. Zhang, G. W. Kattawar, S. G. Warren, B. A. Baum, H. L. Huang, Y. X. Hu, D. Winker, and J. Jaquinta (2008b), Effect of cavities on the optical properties of bullet rosettes: Implications for active and passive remote sensing of ice cloud properties, *J. Appl. Meteorol. Climatol.*, *47*(9), 2311–2330, doi:10.1175/2008JAMC1905.1.
- Yurkin, M. A., V. P. Maltsev, and A. G. Hoekstra (2007), The discrete dipole approximation for simulation of light scattering by particles much larger than the wavelength, *J. Quant. Spectrosc. Radiat. Transfer*, *106*(1–3), 546–557, doi:10.1016/j.jqsrt.2007.01.033.